Research Article

Halima Zidane, Ridha Ben Salem, Abdelkrim Rebiai*, Ghayth Rigane*, Djihad Chenna, Abdelatif Aouadi, Mohammad Al Diab Al Azzawi, Sabry Mohamed Attia, Sheikh Fayaz Ahmad, Maria Atanassova, and Mohammed Messaoudi

Green synthesis of copper oxide nanoparticles from Algerian propolis: Exploring biochemical, structural, antimicrobial, and anti-diabetic properties

https://doi.org/10.1515/gps-2024-0222
received October 09, 2024

Abstract: The green synthesis of nanoparticles (NPs) using natural extracts offers an eco-friendly alternative to traditional methods. In this study, we synthesized copper oxide nanoparticles (CuO NPs) using propolis extract as a natural reducing agent, resulting in two variants: CuO A and CuO B (calcined). UV-Vis spectroscopy confirmed successful synthesis, revealing distinct optical properties influenced by thermal treatment. Fourier transform infrared (FTIR) spectroscopy was performed to identify bioactive compounds stabilizing the NPs, with Cu–O stretching bands at 603 cm^{-1} for CuO A and at 633.6, 596.4, and 484.6 cm^{-1} for CuO B. X-ray diffraction determined crystallite sizes of 68.5 nm (CuO A) and 74.82 nm (CuO B). Scanning electron microscopy showed spherical shapes for CuO A and star-shaped forms for CuO B. Biological assays revealed superior antioxidant activity for CuO A (IC_{50} = 0.027, AEAC = 2.01) compared to CuO B (IC_{50} = 0.052, AEAC = 1.76). CuO A also demonstrated higher total antioxidant capacity (TAC = 11.28 mg EAA/g NPs) and antimicrobial efficacy, with lower minimum inhibitory concentration (MIC = 5–10 $mg{\cdot}mL^{-1}$) than CuO B (MIC = 20–80 $mg{\cdot}mL^{-1}$). Its enhanced glucose absorption capacity highlights its potential antidiabetic applications. These findings underscore the superior biological properties of CuO A, demonstrating its promising biomedical potential.

Keywords: copper oxide, propolis, nanoparticle synthesis, antioxidant, antibacterial, anti-diabetic

*** Corresponding author: Abdelkrim Rebiai,** Laboratory of Applied Chemistry and the Environment, University of El Oued, B.P.789, 39000, El-Oued, Algeria, e-mail: rebiai-abdelkrim@univ-eloued.dz, tel: +213 665487559
*** Corresponding author: Ghayth Rigane,** Laboratory of Organic Chemistry LR17ES08, Sciences Faculty of Sfax, University of Sfax, B.P 1171, 3038 Sfax, Tunisia; Chemistry-Physics Department, Sciences and Technology Faculty, University of Kairouan, B.P 380, Sidi Bouzid, 9100, Tunisia, e-mail: ghaythrigane@gmail.com
Halima Zidane: Laboratory of Organic Chemistry LR17ES08, Sciences Faculty of Sfax, University of Sfax, B.P 1171, 3038 Sfax, Tunisia; Laboratory of Applied Chemistry and the Environment, University of El Oued, B.P.789, 39000, El-Oued, Algeria
Ridha Ben Salem: Laboratory of Organic Chemistry LR17ES08, Sciences Faculty of Sfax, University of Sfax, B.P 1171, 3038 Sfax, Tunisia
Djihad Chenna: Medical Analysis Laboratory of El Medjed, El Oued, Algeria
Abdelatif Aouadi: Laboratory of Applied Chemistry and the Environment, University of El Oued, B.P.789, 39000, El-Oued, Algeria; Process Engineering Laboratory, Applied Sciences Faculty, Kasdi Merbah University, Ouargla, 30000, Algeria
Mohammad Al Diab Al Azzawi: Faculty of Medicine, National Ribat University, Khartoum, Sudan
Sabry Mohamed Attia, Sheikh Fayaz Ahmad: Department of Pharmacology and Toxicology, College of Pharmacy, King Saud University, Riyadh, 11451, Saudi Arabia
Maria Atanassova: Scientific Consulting, Chemical Engineering, University of Chemical Technology and Metallurgy, Sofia, 1734, Bulgaria
Mohammed Messaoudi: Nuclear Research Centre of Birine, Ain Oussera, Djelfa, 17200, Algeria

1 Introduction

Green synthesis of nanoparticles (NPs) has gained attention due to their eco-friendliness and sustainable approach. It involves utilizing natural sources and eco-friendly reducing agents to synthesize NPs [1]. This method has several advantages: low cost, scalability, and no harmful waste production. By employing green synthesis methods, researchers can effectively control the size, shape, and composition of NPs, leading to the development of novel materials with unique properties and diverse applications [2].

Recently, metallic NPs have attracted great interest because of their unique physical and chemical properties.

Their properties can be controlled depending on the synthesis method. One of the main effects, enhanced by controlling particle size, is their antimicrobial action [3,4]. The antimicrobial activity of NPs is a function of surface area in contact with microorganisms. For this reason, the high surface area of NPs assures a wide range of reactions on the surface of microorganisms, inhibiting the normal function of cells or causing cell death [5].

In recent years, significant attention has been paid to metal oxide NPs, particularly copper oxide (CuO) [6]. CuO is a metal-based NP with remarkable antibacterial properties. It is easy to synthesize, cost-effective, heat-resistant, and stable, making it a suitable candidate for metal-based NPs [7]. The antimicrobial activity of CuO is attributed to three primary mechanisms: the release of copper ions, interaction with copper NPs, and inhibition of biofilm formation. CuO exerts its antimicrobial effect through membrane disruption and producing reactive oxygen species (ROS), leading to cellular damage and death in microorganisms [8].

In addition to its antibacterial properties, CuO has garnered interest for its potential applications in addressing metabolic disorders such as diabetes mellitus. Diabetes mellitus is a severe and complex metabolic disorder characterized by chronic hyperglycemia, either due to insufficient insulin production (Type I) or ineffective insulin utilization (Type II). This condition is becoming increasingly prevalent due to lifestyle changes and environmental factors. Inefficient glucose metabolism in diabetic patients often produces excessive hepatic glucose synthesis via glucagon action [9]. Recent research has highlighted the significant role of metals, such as vanadium, chromium, magnesium, and zinc, in regulating blood sugar levels, making them valuable components in diabetes management strategies [10]. These findings suggest that CuO NPs could also contribute to novel therapeutic approaches for diabetes.

However, the effectiveness of NPs, including CuO, as antibacterial and therapeutic agents depends on factors such as particle size, morphology, concentration, exposure time, biocompatibility, and pH [11]. The synthesis process plays a critical role in determining these NP properties and potential applications, emphasizing the importance of adopting green synthesis techniques to optimize their functionality [12].

Propolis, a natural substance collected by bees from various plant sources, has emerged as a widely used natural reducing and stabilizing agent. Its unique chemical composition, including hydroxyl, carbonyl, and amine functional groups, effectively reduces metal ions to nanometer-scale dimensions [13]. Propolis is also well known for its diverse pharmacological properties, including antioxidant, anti-inflammatory, anticancer, and antimicrobial effects. Variations in propolis composition, influenced by geographical region, climate, and collection season [14,15], make it a versatile natural material with over 300 identified bioactive compounds [16].

Several studies have demonstrated the utility of propolis extracts in the synthesis of NPs, such as silver [17], gold [18], palladium [19], and selenium [20]. These studies primarily focus on the antimicrobial [21], anticancer [22], and catalytic [23] properties of the synthesized NPs. However, there is a notable gap in the literature regarding the green synthesis of metal oxide NPs, particularly CuO.

This study presents a distinguished scientific contribution to the green synthesis of metal oxide NPs, focusing on producing CuO NPs using Algerian propolis as an innovative and efficient natural source. Propolis was selected for its unique chemical properties, making it an exceptional reducing and stabilizing agent. It is enriched with active functional groups, such as hydroxyl, carbonyl, and amine, effectively reducing copper ions and converting them into stable NPs with superior functional characteristics. Furthermore, propolis is a sustainable natural material containing biologically active compounds, such as flavonoids and phenolic acids, which endow the resulting NPs with extensive biological potential.

The synthesized CuO NPs represent a significant advancement in medical applications. They exhibit antibacterial properties based on advanced mechanisms, including the generation of ROS and the disruption of microbial cell membranes. Moreover, the study highlights the promising potential of these NPs in enhancing glucose metabolism and regulating blood sugar levels, paving the way for the development of innovative therapeutic solutions for infectious diseases and metabolic disorders, particularly diabetes.

This study is not merely a step toward environmental sustainability through reducing chemical waste. It also constitutes a qualitative leap in developing nanotechnological approaches with diverse medical and environmental applications, positioning it as a model for sustainable nanotechnology.

2 Materials and methods

2.1 Chemicals and reagents

The chemicals and reagents used in this study were sourced from Biochem Chemopharma. They included copper(II) sulfate pentahydrate ($CuSO_4{\cdot}5H_2O$, 99.5%), sodium hydroxide (NaOH, 97%), deionized water (DIW), absolute ethanol (C_2H_5OH, 99%), dimethyl sulfoxide (DMSO, 99.9%), 2,2,2-diphenyl-1-picrylhydrazyl (DPPH, $C_{18}H_{12}N_5O_6$), methanol (CH_3OH, 99.9%), TPTZ

(2,4,6-tris(2-pyridyl)-1,3,5-triazine), hydrochloric acid (HCl, 37%), acetic acid (CH_3COOH, 99.5%), sodium acetate ($CH_3COONa{\cdot}3\ H_2O$, 99%), iron chloride ($FeCl_3$, 99%), and iron sulfate ($FeSO_4$).

The propolis sample used in this study was collected from the Relizane region of Algeria during the summer of 2022. Relizane, located in the northwest of Algeria, boasts a rich and diverse flora, contributing to this region's unique composition of propolis. The collection followed ethical guidelines, ensuring minimal disruption to the bee colonies and adherence to sustainable harvesting practices.

2.2 Propolis extract preparation

Propolis was extracted using a modified version of an established technique, incorporating minor adjustments to enhance the efficiency and quality of the extraction process [24,25]. To prepare the propolis extract, 10 g of finely chopped propolis is combined with 100 mL of 70% ethanol and 30% water solvent solution in a glass container. The mixture is left to soak for precisely 24 h at room temperature in the dark, with continuous agitation. After the soaking period, the solvent solution containing the extracted propolis is collected. This extraction process is repeated three times consecutively to ensure thorough extraction of the propolis components. The solvent solution is collected and concentrated using a rotary evaporator to remove the solvent. Finally, the resulting concentrated extract is stored in a refrigerator at 4°C until further use.

2.3 Green synthesis of copper oxide NPs (CuO NPs)

Green CuO NPs were synthesized using a previously established method, with slight modifications to optimize the process [26]. CuO NPs were synthesized by reducing copper sulfate using phenolic compounds extracted from propolis. The reaction mixture was prepared by combining 100 mL of 0.1 M $CuSO_4{\cdot}5\ H_2O$ solution in a 250 mL flask. The pH of the solution was adjusted to 9 using a suitable base. During the synthesis process, the propolis extract solution ($1\ mg{\cdot}mL^{-1}$) was added slowly in batches using a burette until the desired amount of extract was reached (80 mL). This slow addition allowed for precise control over the reaction and facilitated optimal NP formation.

The biosynthesis reaction was conducted at 40°C for 24 h under controlled conditions. CuO formation was verified by observing a distinct color transition from green to dark brown in the reaction mixture. The resultant brown solid was harvested through centrifugation at room temperature, followed by multiple washes with distilled water and absolute ethanol at 4,500 rpm to remove any unreacted species or impurities. Subsequently, the product was

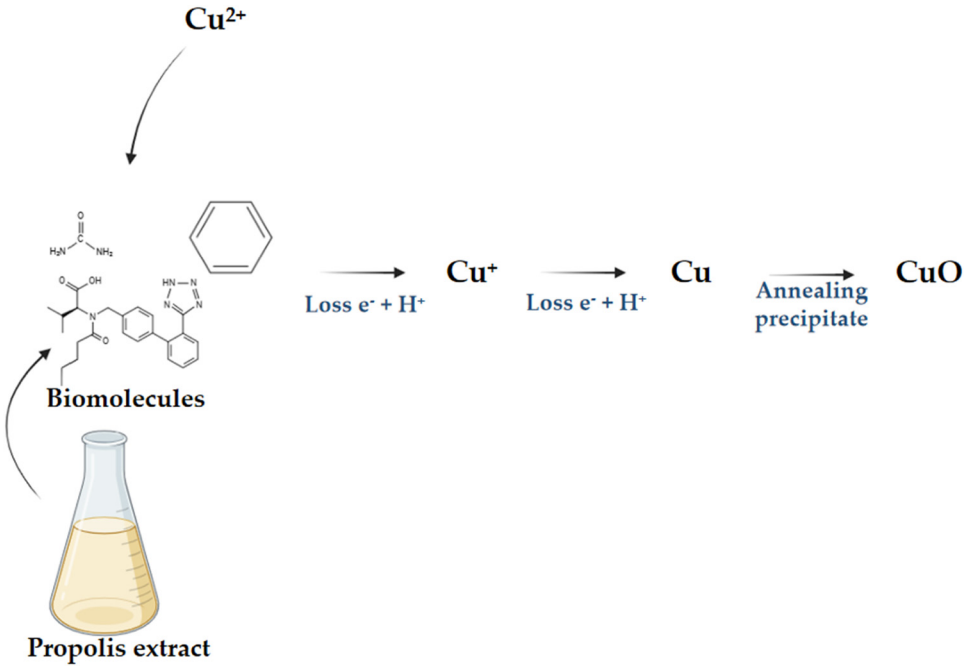

Figure 1: Mechanism of formation of CuO NPs.

subjected to overnight drying at 60°C to remove residual moisture. Half of the obtained quantity underwent further treatment in an oven at 500°C for 4 h to enhance crystallinity and remove organic residues (Figure 1).

2.4 Characterization of CuO NPs

2.4.1 UV-visible spectroscopy

UV-visible spectroscopy is a widely utilized technique for confirming the formation of NPs and assessing their optical properties. The surface plasmon resonance of the spectra is sensitive to particle size, shape, and composition, making it an effective tool for characterizing NP formation [27]. UV-visible spectroscopy was employed to confirm the formation of CuO NPs. The analysis was conducted using a UV-visible spectrophotometer (Shimadzu 1800, Japan) operating within the 200–900 nm wavelength range. This analysis was conducted in a quartz cell, with distilled water as the reference solvent.

2.4.2 FTIR spectroscopy of the synthesized NPs

FTIR spectroscopy is a valuable technique for analyzing the synthesized NPs. It provides information about the vibrational frequencies between the atoms within the NPs. This technique is particularly useful for qualitative analysis, as the intensity of the peaks in the FTIR spectra directly reflects the nature of the materials present [28].

For FTIR analysis, the samples were analyzed using an Agilent Cary 660 Fourier transform infrared spectrophotometer equipped with a Pike MIRacle attenuated total reflection assembly featuring a ZnSe crystal and a liquid nitrogen-cooled linearized mercury cadmium telluride (MCT) detector (Agilent Technologies, Wilmington, DE, USA). Data were collected using Agilent Resolutions software (v. 5.2 and 5.3). Spectra were obtained over wavenumbers ranging from 4,000 to 400 cm^{-1}.

2.4.3 X-ray diffraction (XRD)

The investigation into the structure and grain size of CuOs was conducted using XRD techniques, employing a Cu-Kα (λ = 1.5406 Å) source. The XRD analysis encompassed 2θ angles from 10° to 80°, providing comprehensive coverage of the diffraction patterns. XRD analysis was carried out using a Mini Flex 600 X-ray diffractometer (Rigaku Co. Ltd., Tokyo, Japan), a widely used instrument for material characterization.

2.4.4 Scanning electron microscopy (SEM) and energy-dispersive X-ray spectroscopy (EDX)

SEM is one of the most important techniques for determining morphological characteristics without destroying the structure of the analyzed sample. SEM provides detailed data on the surface characteristics of materials and chemical composition characterization [29].

SEM analysis was conducted using a Zeiss EVO 15 scanning electron microscope equipped with an energy-dispersive X-ray spectroscope (Zeiss, Oberkochen, Germany). This allows for elemental identification and quantitative compositional information of the synthesized NPs.

2.5 Antioxidant properties of the synthesized NPs

2.5.1 Determination of antioxidants by the DPPH assay

The antioxidant or radical scavenging activity of the NPs was assessed using the DPPH assay method. This assay is based on the ability of antioxidants (CuO NPs A/CuO NPs B) to scavenge DPPH free radicals and is commonly used to evaluate the antioxidant capacity of various substances [30].

In this assay, 1 mL of a methanolic solution containing 0.1 mM DPPH was mixed with varying concentrations of CuO NPs A/CuO NPs B (1 mL). The resulting mixture was incubated in darkness for 30 min at room temperature to allow for the reaction between the NPs and the DPPH radicals. After incubation, the absorbance of the reaction mixture was measured at 517 nm using a spectrophotometer against a control comprising 1 mL of water and 1 mL of DPPH solution.

The percentage of inhibition of DPPH radicals by the NPs was calculated using the following equation:

$$\text{DPPH radical scavenging activity (\%)} = (A_{\text{control}} - A_{\text{test}})/A_{\text{control}}) \times 100$$

where A_{control} is the absorbance of the DPPH radical, and A_{test} is the absorbance of the DPPH radical + sample/standard.

The antiradical activity is quantified by the IC_{50} value, which represents the sample concentration required to achieve a 50% reduction in the reduced form of the DPPH radical.

2.5.2 Ferric-reducing antioxidant power assay (FRAP)

The reducing power of ferric ions was assessed using the FRAP method, as described by Benzie and Strain [31]. This method relies on the ability of antioxidants present in CuO NPs A/CuO NPs B to facilitate the conversion of ferric ions (Fe^{3+}) to ferrous ions (Fe^{2+}), which is monitored by the change in color from yellow (Fe^{3+}) to blue (Fe^{2+}).

For the FRAP assay, an FRAP solution was prepared by combining 2.5 mL of 10 mM TPTZ (tripyridyl-s-triazine) in 40 mM HCl, 2.5 mL of 20 mM $FeCl_3$, 25 mL of acetate buffer (pH ~ 3.6), and 3 mL of distilled water. Subsequently, 30 µL of the sample containing CuO NPs A/CuO NPs B was mixed with 970 µL of the prepared FRAP solution. The mixture was then incubated for 30 min at 37°C to allow the reaction to proceed.

The progress of the reaction was monitored using UV-visible spectroscopy by measuring the absorbance at a wavelength of 593 nm [31]. The increase in absorbance indicates the reduction of ferric ions to ferrous ions by the antioxidant properties of the NPs. The FRAP assay provides valuable information about the ferric-reducing power of CuO NPs A/CuO NPs B, reflecting their antioxidant capacity.

2.5.3 Total antioxidant capacity (TAC)

The TAC of the NPs was determined using the phosphomolybdenum method, a widely recognized technique for assessing the antioxidant potential [30,32]. This method is based on the reduction of molybdenum Mo (VI) in the form of molybdate ions (MoO_4^{2-}) to molybdenum Mo(V) (MoO_2^{+}) in the presence of an antioxidant. The reduction process results in the forming of a green phosphate/Mo(V) complex under acidic pH conditions.

To conduct the assay, 0.2 mL of each sample was mixed with 2 mL of a reagent solution composed of 0.6 M sulfuric acid, 28 mM sodium phosphate, and 4 mM ammonium molybdate. The reaction tubes were securely sealed and incubated at 95°C for 90 min to ensure reaction completion. Following the incubation period, the absorbance of the reaction solutions was measured at 695 nm using a spectrophotometer, with distilled water serving as the blank reference. The absorbance values were recorded after cooling.

2.6 Antibacterial activity of the NPs

The minimum inhibitory concentration (MIC) and minimum bactericidal concentration (MBC) of CuO A NPs and CuO B NPs were determined using the broth microdilution method in sterile 96-well flat-bottom microplates (Nunc, USA), with a final volume of 150 µL per well, as described in the study of Balouiri et al. [33] with minor modifications. Bacterial strains (*Escherichia coli, Pseudomonas aeruginosa, Staphylococcus aureus,* and *Bacillus subtilis*) and the fungal strain (*Candida albicans*) were cultured in Mueller–Hinton broth (MHB) and Sabouraud dextrose broth (SDB), respectively. The bacterial inoculum was prepared by diluting the bacterial culture in MHB to achieve a final concentration of approximately 5×10^5 CFU·mL^{-1} (McFarland standard 0.5), which was further diluted 1:100 with broth and added (75 µL) to each well along with 75 µL of the corresponding nanoparticle suspension. The fungal inoculum was diluted to a final concentration of 10^6 CFU·mL^{-1} in SDB. Serial dilutions of CuO NPs were prepared in each well using sterile MHB for bacterial strains and SDB for fungal strains. The following concentrations were tested: 16, 8, 4, 2, 1, 0.5, 0.25, 0.125, 0.0625, and 0.031 mg·mL^{-1}. Control wells included a growth control (no NPs), a sterile control (broth only), and a microbial control (bacterial or fungal suspension without NPs). The plates were incubated at 37°C for 18–24 h for bacterial strains and 48 h for fungal strains. After incubation, microbial viability was assessed by adding 10 µL of resazurin dye (337.5 mg of resazurin powder in 50 mL of sterile distilled water; Serva, Germany) to each well. The plates were then incubated at 37°C for 3 h to observe color changes, indicating microbial growth or inhibition. The MIC was determined as the lowest concentration of CuO NPs that completely inhibited visible microbial growth (the last well to remain purple before turning pink).

For MBC determination, 3 µL of samples were taken from wells with no visible growth and spread onto Mueller–Hinton agar (for bacteria) or Sabouraud dextrose agar (for fungi). The plates were incubated at 37°C for 18–24 h for bacterial strains and 48 h for fungal strains. The MBC was defined as the lowest concentration of CuO NPs, resulting in ≥99.9% reduction in microbial growth.

The MIC and MBC values were expressed as the arithmetic mean of triplicate tests with the standard deviation. Bactericidal activity was classified based on the MBC/MIC ratio: if the ratio was ≤4, the effect was considered bactericidal; if the ratio was >4, the effect was considered bacteriostatic.

2.7 Anti-diabetic activity assessed by glucose uptake in yeast cells

Commercial baker's yeast (*Saccharomyces cerevisiae*) was washed by repeated centrifugation at 3,000 × *g* for 5 min

with distilled water until the supernatant became clear. A 10% yeast suspension (v/v) was then prepared in distilled water. Various concentrations of CuO NPs (CuONPs A and CuONPs B), ranging from 1.5 to 48 mg·mL^{-1}, were added to 1 mL of a glucose solution (25 mM or 4.5039 g·L^{-1}), followed by incubation for 10 min at 37°C. The reaction was initiated by adding 100 µL of the prepared yeast suspension to the glucose solution. The mixture was vortexed and further incubated at 37°C for two time points: 30 min (T30) and 120 min (T120). After incubation, the reaction mixture was centrifuged at 2,500 × *g* for 5 min, and the glucose concentration in the supernatant was measured. Glucose levels were determined by absorbance at 540 nm. All experiments were performed in triplicate to ensure the accuracy and reproducibility of the results [34].

3 Results and discussion

3.1 UV-visible spectroscopy

This study focuses on the rapid and environmentally friendly synthesis of CuO NPs using propolis extract. Propolis is widely recognized for its rich composition of bioactive compounds, including phenolic acids, flavonoids, terpenes, bioelements, vitamins, proteins, and amino acids. Among these, gallic acid has been identified as a major phenolic compound within propolis extract [35], playing a potentially critical role as a catalyst in the reduction of $Cu(OH)_2$ to nanoscale CuO.

As depicted in Figure 2, the prominent absorption peaks at 259, 284, 301, and 325 nm in the UV-Vis spectrum of the crude *Relizane propolis* extract indicate the presence of polyphenols and flavonoids [36]. The observed color shift from blue to brown can be attributed to the excitation of surface plasmon resonance coupled with the antioxidant activity of polyphenols. This color transition, driven by $\pi \rightarrow \pi^*$ electronic transitions, confirms the successful synthesis of CuO NPs [37].

The UV-Vis spectrum of CuO NPs synthesized from propolis (CuO NPs A) reveals two absorption bands at 314 and 370 nm, whereas calcined CuO NPs (CuO NPs B) exhibit a broader absorption peak centered at 355 nm, corresponding to the surface plasmon absorption of the metal oxide, as illustrated in Figure 2. Surface plasmon absorption in metal oxide NPs arises from the collective oscillation of free conduction band electrons induced by incident electromagnetic radiation. This resonance effect becomes pronounced when the wavelength of the incident light significantly exceeds the particle diameter [38].

3.2 FTIR analysis

FTIR analysis was employed to identify the potential biomolecules present in propolis extract responsible for reducing Cu ions to cuprous oxide NPs. The analysis was conducted within the spectral range of 400–4,000 cm^{-1}. This allowed us to gain insights into how the propolis extract functions as both a reducing and capping agent, influencing the formation of new functional groups and biomolecules attached to the surface of CuO NPs.

As shown in Figure 3, the propolis extract exhibited a spectral profile characterized by 14 distinct peaks at specific wavenumbers (3,403.9, 2,912.9, 2,752.6, 2,092.9, 1,906.5,

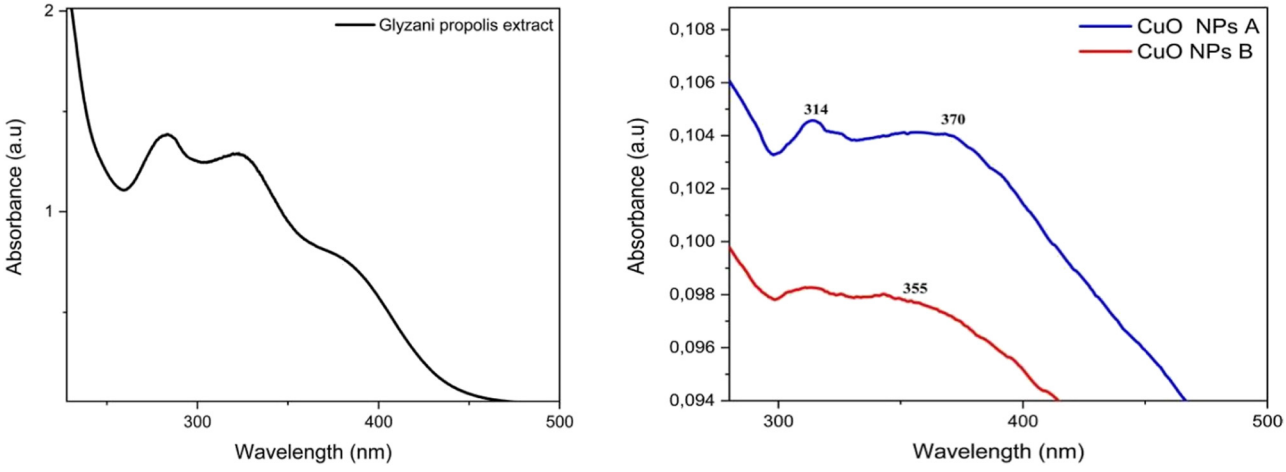

Figure 2: UV-visible spectra of CuO NPs and propolis extract.

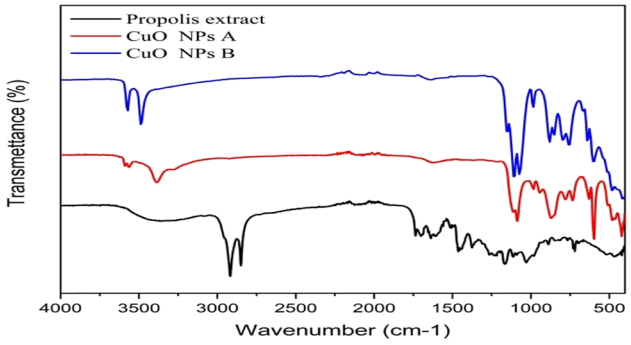

Figure 3: FTIR spectral characterization of propolis extract and synthesized CuO NPs (A and B).

1,707.1, 1,623.3, 1,442.5, 1,351.2, 1,246.8, 1,172.2, 1,021.3, 713.8, and 475.2 cm^{-1}). However, it is noteworthy that these peaks underwent shifts in their positions and alterations in their intensities following the formation of CuO NPs.

The IR spectrum of CuO NPs A using propolis extract showed a peak corresponding to O–H stretching frequencies of 3,559.6 cm^{-1}, confirming the presence of OH groups from alcohols and phenol. Nonetheless, evidence suggests that the peak at 3,384.4 cm^{-1} can be attributed to the stretching vibration of the N–H group [39]. The peaks at 2,930–2,850 cm^{-1} (at approximately 2,912.9 cm^{-1}) are assigned to the asymmetric stretching of methylene, and the peaks at approximately 2,752.6, 2,092.9, and 1,906.5 cm^{-1} are assigned to the symmetric stretching of the hydrocarbons [40]. This peak was shifted to wavenumbers of 2,294.2 and 2,085.4 cm^{-1} after CuO NPs A synthesis (Figure 3). Absorptions at 1,707.1, 1,623.3, and 1,442.5 cm^{-1} corresponding to the carbonyl C═O stretching vibration of flavonoids and lipids are found in the propolis. This peak was shifted to a wavenumber of 1,613.9 cm^{-1} and was assigned to the bending vibrations of the carbonyl group, indicating the presence of flavonoids adsorbed on the surface of the biosynthesized CuO NPs A. The bands at 1,351.2 and 1,246.8 cm^{-1} were due to the C–O–H stretching vibration, and the band at 1,172.2 cm^{-1} was considered to occur due to the presence of lipids and alcohol groups (stretching of C–O and bending of C–OH), and the band at 1,021.3 cm^{-1} was attributed to the stretching of the aromatic ether C–O–C bonds [41,42]. This peak was shifted to a wavenumber of 1,099.6 cm^{-1} and was due to the C–O stretching vibrations of the carboxylic group and flavanones. The peak at 713.8 cm^{-1} may be related to the vibration of the aromatic rings; after the synthesis of CuO NPs, this peak undergoes a noticeable shift to wavenumbers of 872.2 and 756.6 cm^{-1}. Moreover, a pronounced and intense peak at 603.8 cm^{-1} can be attributed to the stretching vibration of Cu–O bonds. This peak strongly supports the formation of CuO A NPs [43].

Moreover, the IR spectrum of calcined CuONPs B displayed broad peaks corresponding to the O–H stretching frequencies at 3,570.8 and 3,488.8 cm^{-1}, confirming the presence of the OH group derived from alcohols and phenols. The peaks at 1,110.7 and 1,073.5 cm^{-1} were attributed to C–O stretching vibrations of the carboxyl group and flavanones, consistent with previous reports [39,44]. Five IR absorption peaks in calcined CuO nanostructures show the 700–400 cm^{-1} vibrational mode. The bands at 633.6, 596.4, and 484.6 cm^{-1} corresponded to the vibrations of the Cu–O band, confirming the synthesis of CuO NPs B [45].

The FT-IR spectrum confirmed the role of different functional groups in propolis extract, such as phenolic acids, flavonoids, terpenes, bioelements, and other components, such as vitamins, proteins, amino acids, and sugars, in reducing Cu^{2+} to form CuO NPs, followed by capping the surface of the final product to increase its stability.

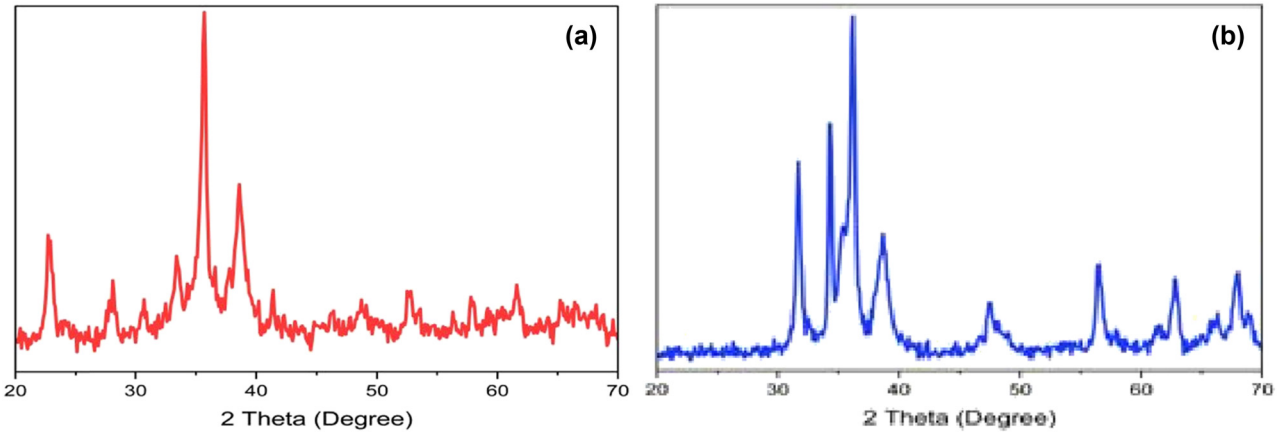

Figure 4: XRD patterns of NPs synthesized from propolis extract: (a) CuO NPs and (b) calcined CuO NPs.

3.3 XRD analysis

Figure 4a presents the XRD pattern of CuO NPs A. A weak diffraction peak at 41.3° is observed, originating from the copper foil substrate (JCPDS 04-0836). Additionally, distinct peaks were identified at angles 22.9°, 30.9°, 33.6°, 38.5°, 48.9°, 58°, 61.7°, and 63.4°, corresponding to the (021), (110), (002), (200), (020), (202), (-113), and (200) Miller planes, respectively. The peaks at 52.9° and 66.6° are attributed to crystalline and amorphous organic phases. These diffraction peaks' positions and relative intensities align well with standard XRD data for $Cu(OH)_2$ NPs (JCPDS file No. 35-0505). Additionally, distinct peaks are identified at angles 35.7°, 56.5°, and 68.1°, corresponding to the (111), (151), and (220) Miller planes, respectively, which were consistent with the standard XRD data for CuO NPs (JCPDS 48-1548) and Cu_2O NPs (JCPDS file No. 05-0667).

Figure 4b shows the XRD pattern of CuO NPs B. Notably, many peaks corresponding to crystalline and amorphous organic phases and peaks of CuO NPs A are absent, while others become clearer and more prominent. The peaks observed at angles 31.8°, 36.1°, 47.5°, 56.6°, 62.8°, 66.2°, and 68.8° correspond to the (110), (111), (−202), (151), (200), (-311), and (220) Miller planes, respectively. Moreover, the peaks at 34.4°, 38.7°, and 61.2° are associated with the (002), (022), and (−113) Miller planes, respectively, consistent with standard XRD data for CuO NPs (JCPDS 48-1548) and Cu_2O NPs (JCPDS file No. 05-0667).

The crystalline size was determined using the Debye–Scherrer formula:

$$D = \frac{k\lambda}{\beta \cos\theta}$$

where $k = 0.9$, β represents the full width at half-maximum of the XRD peak, and θ is the Bragg's angle. The average crystalline sizes of CuO NPs A and CuO NPs B were calculated to be 68.5 and 74.82 nm, respectively.

3.4 SEM and energy-dispersive spectroscopy (EDS)

The surface properties of CuO NPs synthesized using different methods were analyzed via SEM. Figure 5 depicts the SEM analysis of CuO A NPs synthesized from propolis extract at a weight-to-volume ratio of 1:4. The SEM image reveals agglomerated CuO NPs A with spherical shapes. The observed high agglomeration could be attributed to the low percentage of propolis extract used as a stabilizing agent and the polarity of CuO NPs due to the high concentration of precursors. The particles exhibit a spherical shape, forming clumps that appear to be interconnected.

EDS was employed to investigate the chemical composition of CuO NPs A. The SEM-EDS spectra reveal that the sample comprises 64.82% copper, 23.57% oxygen, and 11.61% carbon, consistent with XRD results.

Figure 6 illustrates the SEM analysis of CuO NPs B synthesized from propolis extract at a weight-to-volume ratio of 1:4. The SEM image shows agglomerated CuO NPs B with star shapes. Unlike CuO NPs A, where all particles were interconnected, CuO NPs B form sub-agglomerates, each resembling a star shape with formal symmetry.

Similarly, EDS was employed to determine the chemical composition of CuO NPs B. The SEM-EDS spectra indicate that the sample comprises 88.26% copper, 9.17% oxygen, and 2.56% carbon, consistent with the XRD results. This analysis provides valuable insights into the morphology and elemental composition of the synthesized NPs, shedding light on their structural properties and potential applications.

3.5 DPPH assay

The DPPH assay, depicted in Figure 7, is a crucial method for assessing the antioxidant activity of various compounds by evaluating their capability to scavenge DPPH radicals. The assay results reveal differing antioxidant effects among the tested samples, as shown in Table 1.

Starting with ascorbic acid, which emerges as the most active antioxidant component with the lowest IC_{50} value of 0.021, it functions primarily as a hydrogen donor. Ascorbic acid donates hydrogen atoms from its hydroxyl groups to free radicals, thereby initiating a process that ultimately reduces free radicals to stable non-radical species. This mechanism highlights the effectiveness of ascorbic acid, even against highly potent free radicals.

Following closely, CuO NPs A exhibit an IC_{50} value of 0.027, indicating significant antioxidant potential. This notable effect can be attributed to a synergistic interaction between the copper hydroxide NPs and the bioactive compounds present in propolis. The combined action of these components enhances the overall antioxidant activity observed.

In contrast, CuO NPs B demonstrate a higher IC_{50} value of 0.052, suggesting a relatively weaker antioxidant effect compared to the other samples tested. This weaker effect may stem from the NPs undergoing electron exchange reactions, wherein they either accept or donate electrons to neutralize the radicals. However, this mechanism may not be as efficient in neutralizing the DPPH radicals as the

hydrogen donation mechanism exhibited by ascorbic acid and the synergistic effect observed in CuO A NPs. These findings underscore the importance of NP composition and structure in determining their antioxidant properties.

3.6 FRAP assay

The FRAP assay, depicted in Figure 8, is a valuable method for evaluating antioxidant capacity by measuring the reduction of ferric ions (Fe^{3+}) to ferrous ions (Fe^{2+}) in the presence of antioxidants. The results from this assay provide insights into the antioxidant potential of the tested samples, as shown in Table 2.

Starting with ascorbic acid, which emerges as the most potent antioxidant in this assay, it demonstrates high antioxidant capacity by donating electrons to ferric ions (Fe^{3+}), thereby reducing them to ferrous ions (Fe^{2+}). This process results in the formation of dehydroascorbic acid, which effectively neutralizes harmful free radicals, thus preventing oxidative damage. Ascorbic acid's ability to efficiently donate electrons makes it highly effective in combating oxidative stress.

Similarly, CuO NPs A exhibit a higher antioxidant capacity, as evidenced by their AEAC value of 2.01. This indicates a significant ability to donate electrons and facilitate the reduction of ferric ions. The observed antioxidant capacity of CuO A NPs may be attributed to the presence of

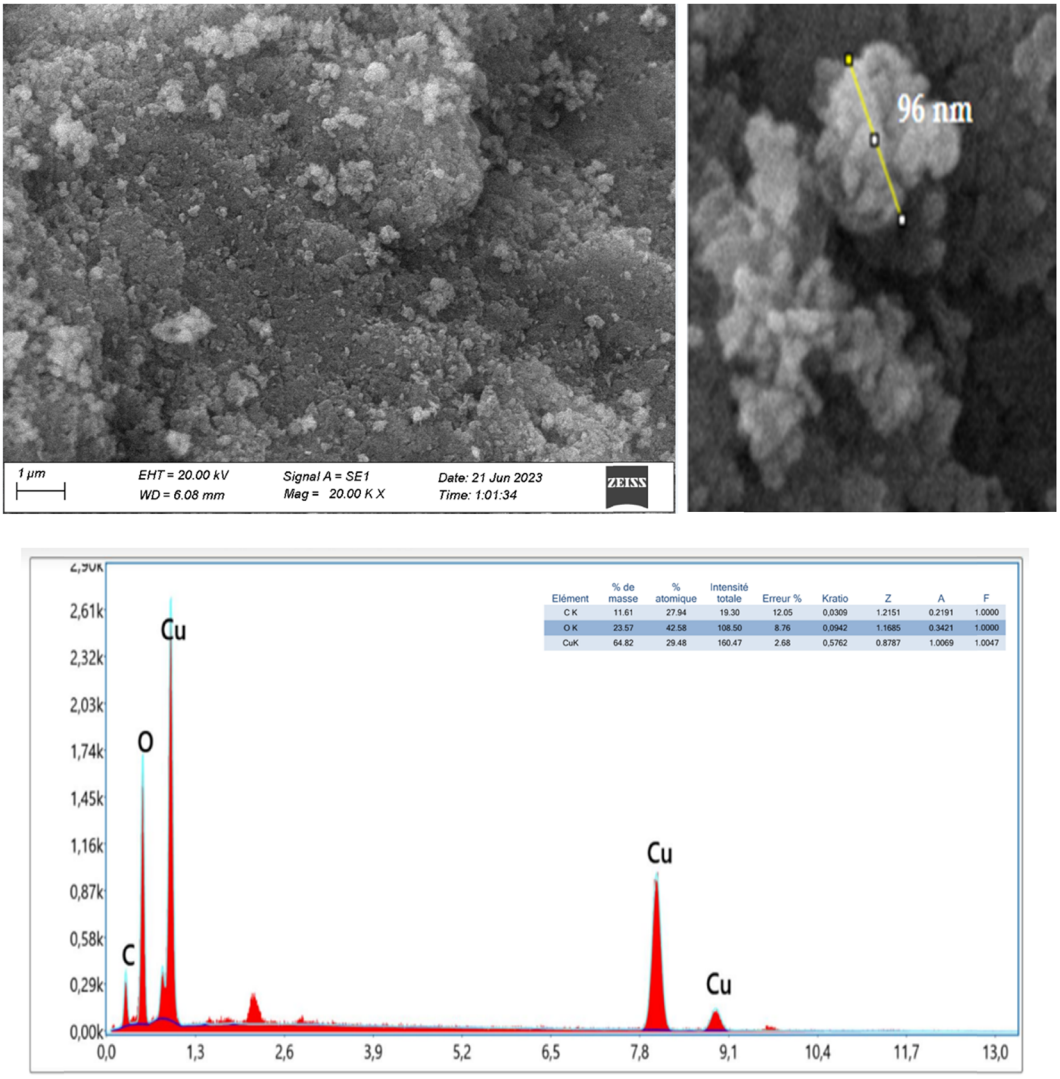

Figure 5: SEM and EDS analysis of CuONPs A synthesized from propolis extract.

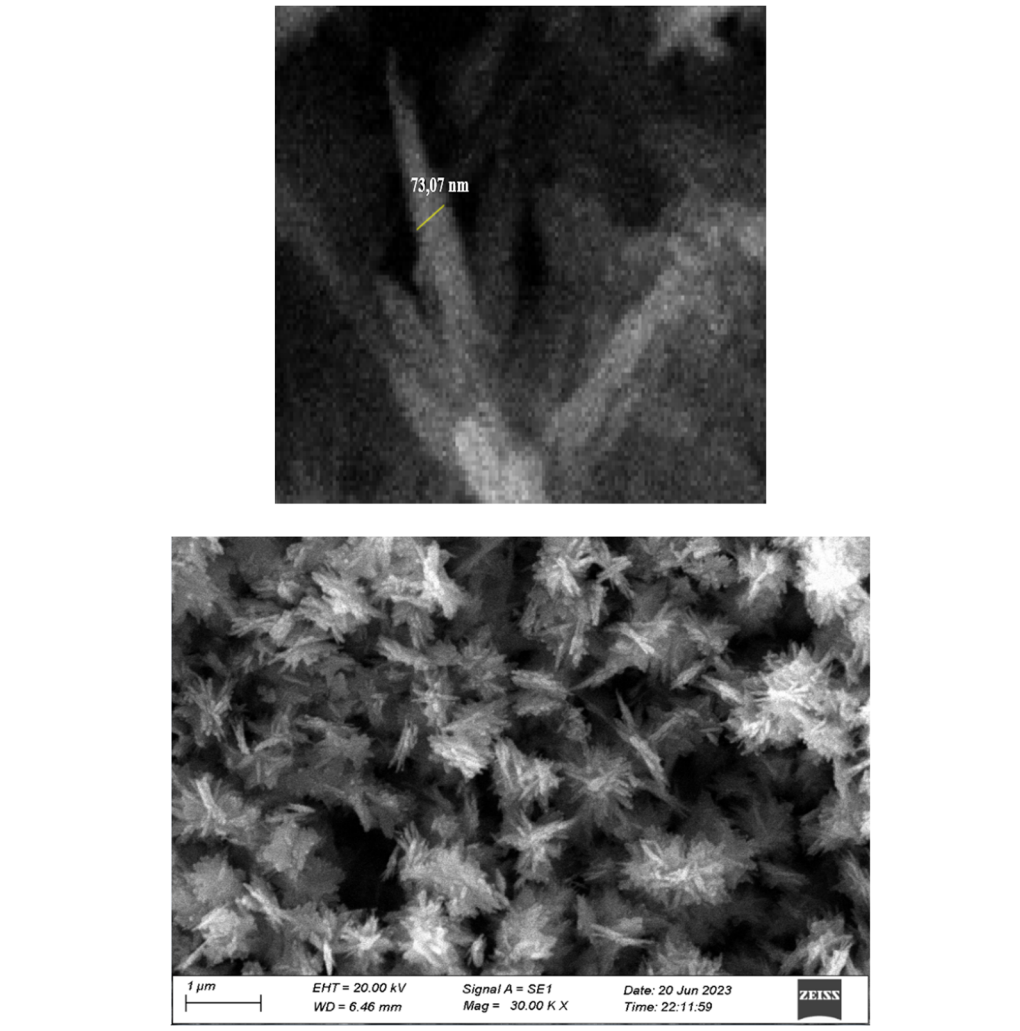

Figure 6: SEM and EDS analysis of calcined CuO NPs B synthesized from propolis extract.

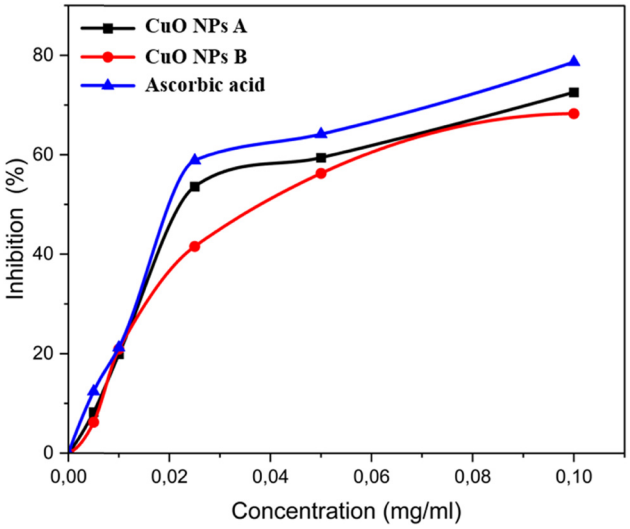

Figure 7: DPPH radical scavenging activity of CuO NPs synthesized from propolis extract.

Table 1: DPPH radical scavenging activity of CuO NPs synthesized from propolis extract

Sample	Ascorbic acid	CuO NPs A	CuO NPs B
IC_{50}	0.021	0.027	0.052

bioactive compounds in propolis, which synergistically enhance the antioxidant activity of copper.

In contrast, CuO NPs B display a lower AEAC value of 1.76, suggesting a reduced capability to reduce ferric ions

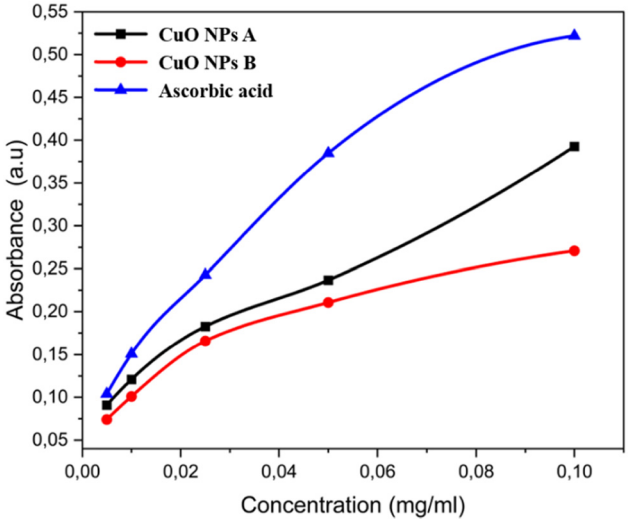

Figure 8: Ferric reducing antioxidant power of CuO NPs synthesized from propolis extract.

Table 2: Ferric reducing antioxidant power of CuO NPs synthesized from propolis extract

Sample	CuO NPs A	CuO NPs B
AEAC	2.01	1.76

compared to CuO NPs A and ascorbic acid. Consequently, CuO NPs B exhibit lower antioxidant capacity in this assay. This difference in antioxidant capacity may stem from variations in the chemical properties and surface reactivity of NPs, affecting their ability to donate electrons and participate in the reduction of ferric ions. These findings underscore the importance of the composition and structure of NPs in determining their antioxidant properties.

3.7 TAC

Figure 9 and Table 3 present the TAC results obtained from the synthesized CuO NPs A and B. The TAC measurements reveal a notable antioxidant capacity in both CuO NPs A and B. Notably, CuO NPs A exhibited the highest antioxidant activity, with a value of 11.28 mg EAA/g NPs.

Copper deficiency adversely affects the body's antioxidant function and predisposes individuals to various diseases. The CuO NPs prepared in this study have the potential to elevate copper levels in the blood of individuals suffering from copper deficiency, consequently enhancing antioxidant activity. Moreover, the impact of CuO NPs extends to cell membranes' composition, thereby fortifying the integrity and functionality of cell membranes, tissues, and organs.

Min et al. [46] investigated the effects of copper oxide (Cu_2O NPs) on the antioxidant function of Cu-deficient

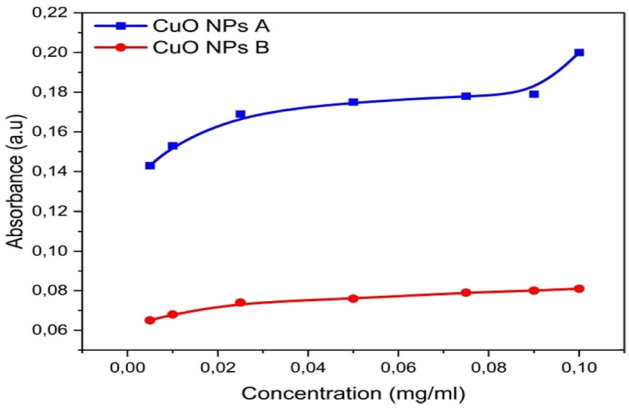

Figure 9: TAC of CuO NPs synthesized from propolis extract.

Table 3: TAC of CuO NPs synthesized from propolis extract

Sample	CuO NPs A	CuO NPs B
TAC (mg EAA/g NPs)	11.28	32.89

Kazakh sheep. They observed significantly lower copper levels in the blood, wool, and liver of Cu-deficient Kazakh sheep compared to healthy animals. To address this deficiency, the authors supplemented Cu-deficient Kazakh sheep with Cu_2O NPs or $CuSO_4$. Consequently, the blood copper concentration notably increased. Interestingly, starting from day 5 of supplementation, the copper content in the Cu_2O groups surpassed that of the $CuSO_4$ group [46].

3.8 Assessing antibacterial activity mediated by NPs

CuO NPs A (Table 4 and Figure 10) demonstrate significantly higher antimicrobial efficacy compared to CuO NPs B (Table 5 and Figure 11), as evidenced by the lower MIC values across the tested strains. For *B. subtilis*, CuO NPs A achieved an MIC of 5 $mg{\cdot}mL^{-1}$, while CuO NPs B required a much higher MIC (20 $mg{\cdot}mL^{-1}$). Similarly, CuONPs A exhibited an MIC of 10 $mg{\cdot}mL^{-1}$ for *E. coli* and *S. aureus* compared to those of 40 $mg{\cdot}mL^{-1}$ and 80 $mg{\cdot}mL^{-1}$, respectively, for CuO NPs B. In the case of *P. aeruginosa*, CuO NPs B displayed very high concentrations (VHC) to inhibit bacterial growth, whereas CuO NPs A managed to achieve inhibition with an MIC of 40 $mg{\cdot}mL^{-1}$. Regarding the fungal strain *Candida albicans*, CuO NPs B were ineffective at standard concentrations, requiring VHC for both MIC and MFC, while CuO NPs A maintained their efficacy with an MIC of 40 $mg{\cdot}mL^{-1}$. These results highlight the superior performance of CuO NPs A as an antimicrobial agent, driven by its compositional and structural advantages compared to CuO NPs B (Table 6).

The observed differences in antimicrobial activity between CuO NPs A and CuO NPs B can be attributed to fundamental variations in their chemical composition and preparation methods. CuO NPs A, synthesized using propolis, incorporate bioactive compounds such as flavonoids and phenolic acids, which synergistically enhance their antimicrobial properties. These compounds promote increased production of ROS, which directly attacks microbial cells by damaging their membranes and interfering with essential intracellular processes [48]. Additionally, CuO NPs A possess superior surface properties, allowing for enhanced interaction with microbial cells. In contrast, CuO NPs B, prepared through calcination, lack these bioactive components, limiting their ability to interact effectively with microbial membranes. This limitation is particularly evident with resistant strains such as *P. aeruginosa* and *C. albicans*, which have thicker and more complex cell walls [49]. Furthermore, the crystallinity and surface structure of CuO NPs B reduce their efficiency in penetrating microbial cells and disrupting their integrity, explaining the higher MIC and MFC values observed.

The antimicrobial activity of CuO NPs is primarily driven by their ability to generate ROS, including hydroxyl radicals and hydrogen peroxide, which play a pivotal role in microbial cell destruction [50]. ROS oxidize membrane lipids and proteins, compromising the structural integrity of microbial cells. Additionally, ROS inflict direct damage on microbial DNA and intracellular proteins, disrupting key processes such as cellular respiration and energy production [51]. CuO NPs A demonstrated superior ROS generation, largely due to the presence of flavonoids and phenolic compounds, which act as chemical and physical catalysts to enhance ROS production. Upon interaction with microbial cell surfaces, CuO NPs induce changes in

Table 4: Broth microdilution assay of CuO NPs A from *E. coli, P. aeruginosa, S. aureus, B. subtilis,* and *C. albicans*

Bacterial strains (*n* = 3)	**Antibacterial activity of CuO NPs A**		
	MIC value ($mg{\cdot}mL^{-1}$)	**MBC value ($mg{\cdot}mL^{-1}$)**	**MBC/MIC ratio**
E. ATCC 25922	10	40	4
P. aeruginosa ATCC 27853	40	80	2
S. aureus ATCC 25932	10	20	2
B. subtilis ATCC 21332	5	10	2
Fungus strain (*n* = 3)	**Anti-Candida activity of CuO NPs A**		
	MIC value ($mg{\cdot}mL^{-1}$)	**MFC value ($mg{\cdot}mL^{-1}$)**	**MFC/MIC ratio**
C. albicans ATCC 10231	40	VHC	—

VHC, very high concentrations; MIC, minimum inhibitory concentration; MBC, minimum bactericidal concentration; MFC, minimum fungicide concentration for a fungus (corresponds to a lethality rate of minimum 99.9%).

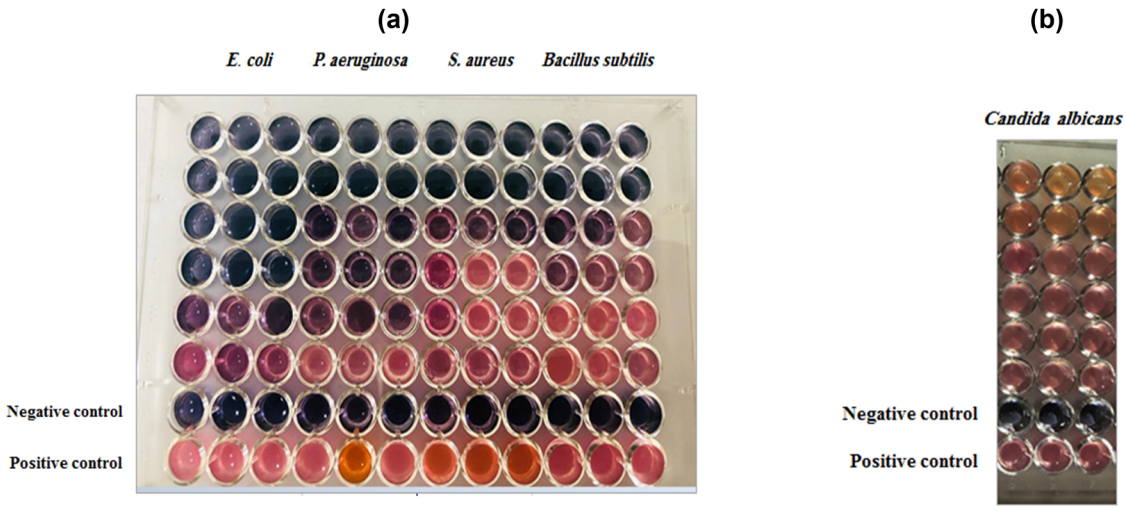

Figure 10: Antimicrobial efficacy of CuO NPs A. Broth microdilution assay shows (a) antibacterial activity against *E. coli*, *P. aeruginosa*, *S. aureus*, and *B. subtilis*, and (b) anti-candida activity against *C. albicans* at concentrations of 80–2.5 mg·mL^{-1}.

Table 5: Broth microdilution assay for CuO NPs B for *E. coli*, *P. aeruginosa*, *S. aureus*, *B. subtilis*, and *C. albicans*

Bacterial strains (*n* = 3)	**Antibacterial activity of CuO NPs B**		
	MIC value (mg·mL^{-1})	**MBC value (mg·mL^{-1})**	**MBC/MIC ratio**
E. coli ATCC 25922	40	80	2
P. aeruginosa ATCC 27853	80	VHC	—
S. aureus ATCC 25932	80	VHC	—
B. subtilis ATCC 21332	20	80	4
Fungus strain (*n* = 3)	**Anti-Candida activity of CuO NPs B**		
	MIC value (mg·mL^{-1})	**MFC value (mg·mL^{-1})**	**MFC/MIC ratio**
C. albicans ATCC 10231	VHC	VH.C	—

VHC, very high concentrations; MIC, minimum inhibitory concentration; MBC, minimum bactericidal concentration; MFC, minimum fungicide concentration for a fungus (corresponds to a lethality rate of minimum 99.9%).

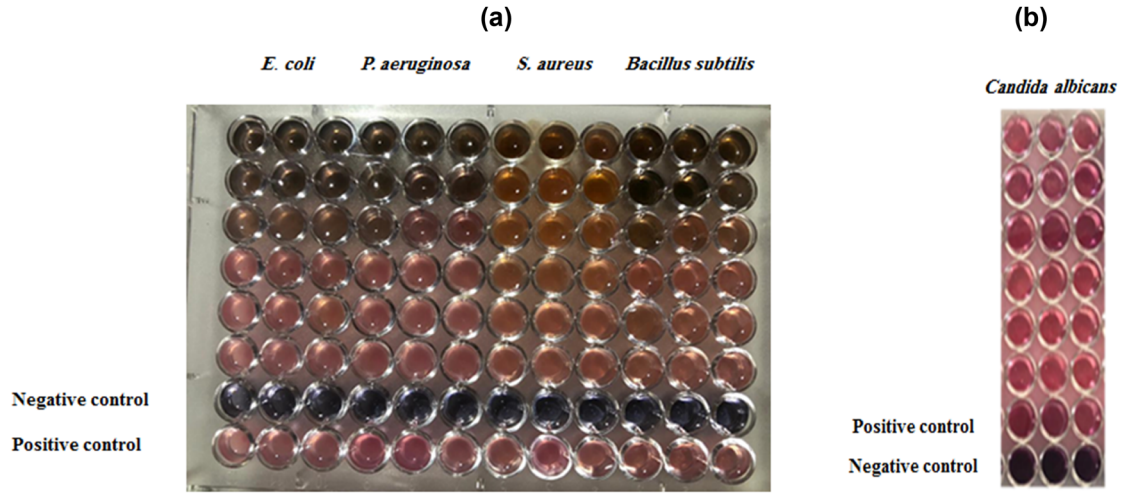

Figure 11: Antimicrobial efficacy of CuO NPs B. Broth microdilution assay showed (a) antibacterial activity against *E. coli*, *P. aeruginosa*, *S. aureus*, and *B. subtilis* and (b) anti-candida activity against *C. albicans* at concentrations of 80–2.5 mg·mL^{-1}.

Table 6: MIC and MBC of selected compounds against various microorganisms: compounds tested were tannic acid, quinine, guaiazulene, and quercetin [47]

	Tannic acid		Quinine		Guaiazulene		Quercetin	
	MIC	MBC	MIC	MBC	MIC	MBC	MIC	MBC
E. coli	1.0 ± 0.0	8.0 ± 0.0	3.3 ± 1.2	5.3 ± 1.9	16.0 ± 0.0	—	16.0 ± 0.0	—
P. aeruginosa	1.0 ± 0.0	—	16.0 ± 0.0	16.0 ± 0.0	16.0 ± 0.0	—	10.7 ± 4.6	—
B. subtilis	0.12 ± 0.00	4.0 ± 0.0	5.3 ± 2.3	16.0 ± 0.0	10.7 ± 4.6	—	8.0 ± 0.0	—
S. aureus	0.25 ± 0.00	1.33 ± 0.57	0.33 ± 0.14	0.58 ± 0.38	16.0 ± 0.0	16.0 ± 0.0	—	—

membrane permeability, facilitating the internalization of NPs into the cytoplasm, where they disrupt essential cellular functions (Figure 12) [52].

In contrast, CuO NPs B exhibited lower efficacy due to their lack of active compounds and limited surface properties. Resistant microorganisms like *P. aeruginosa* and *C. albicans* possess thick and complex cell walls composed of components such as chitin and glucans, making them less susceptible to penetration by less potent NPs like CuO NPs B. However, CuO NPs A, with their enhanced properties, effectively penetrate these barriers and exert antimicrobial action [48].

3.9 Glucose uptake in yeast cells

The mechanism of glucose transport across the yeast cell membrane has garnered significant attention as an *in vitro* screening method for the hypoglycemic effects of various compounds. The findings of this study revealed that calcined CuO NPs A and non-calcined CuO NPs B effectively enhanced glucose uptake in yeast cells. At T30 (Figure 13), the use of CuO NPs A resulted in a significant reduction in extracellular glucose concentration, demonstrating their efficiency in stimulating immediate glucose uptake by yeast cells. Glucose concentrations at CuO NP concentrations (1.5, 3, 6, 12, 24, and 48) were 325, 301, 285, 244, 198, and 172 mg·mL^{-1}, respectively. In contrast, glucose concentrations for CuO NPs B at the same doses were 334, 326, 319, 285, 274, and 258 mg·mL^{-1}, respectively. Both results showed superior performance compared to the negative control, where the glucose concentration was 453 mg·mL^{-1}. The positive control, based on metformin and the drug (MTZ) reported in studies by Pitchaipillai and Ponniah [53], and Pulivarthi et al. [54] demonstrated 95% and 88% efficacy, respectively (Table 7).

The superior performance of CuONPs A can be attributed to their structural properties, such as smaller size and larger surface area, which enhance their interaction with glucose transporters on the cell membrane. At T120 (Figure 14), the NPs exhibited a more sustained effect on glucose absorption, indicating the simultaneous activation of high- and low-

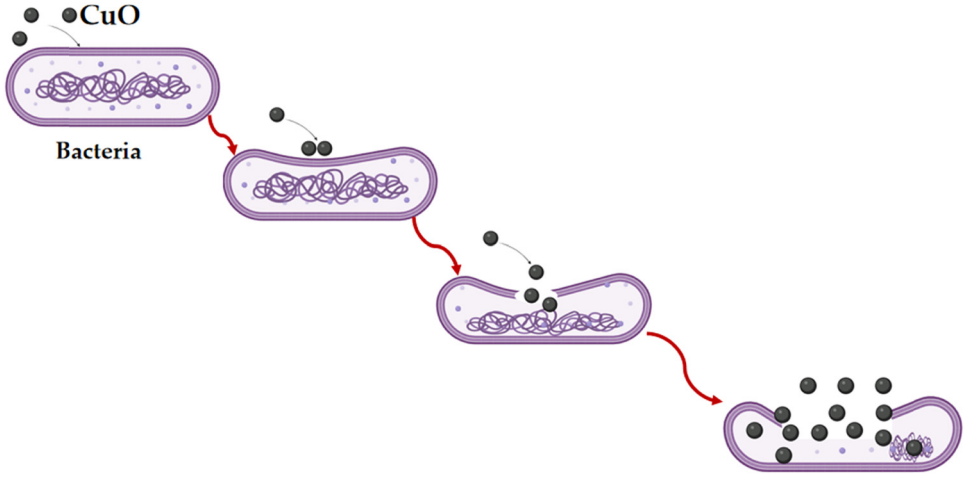

Figure 12: Mechanism of antibacterial activity of CuO NPs.

efficiency glucose transporters, accelerating glucose uptake. At T120 (Table 8), the glucose concentrations at the same doses were 302, 298, 274, 212, 102, and 73 mg·mL^{-1} for CuO NPs A and 319, 308, 306, 285, 274, and 252 mg·mL^{-1} for CuO NPs B. The superior physiological efficacy of CuO NPs A at this stage reflects their enhanced capability to influence cellular processes governing glucose uptake.

This mechanism aligns with recent findings suggesting that sugar transport across the yeast cell membrane is mediated by stereospecific membrane transporters [55]. Specifically, glucose transport in yeast (*S. cerevisiae*) is highly complex, and it is well established that glucose is transported via facilitated diffusion. Facilitated transporters are specific carriers that move solutes along their concentration gradient, crucial in enhancing efficient glucose uptake. The improved glucose uptake, as demonstrated in this study with CuO NPs A, highlights the potential of NPs to enhance glucose utilization, thus promoting the regulation of blood glucose levels.

Recent studies on sugar and non-metabolizable glycoside transport suggest that sugar transport across the yeast cell membrane is mediated by stereospecific membrane transporters [56]. Reports indicate that in yeast cells (*S. cerevisiae*), glucose transport occurs through a complex process, primarily facilitated diffusion. Facilitated transporters are specific carriers that move solutes along their concentration gradient, effectively improving glucose uptake [54]. The increased glucose absorption demonstrated in this study with CuO NPs A underscores the ability of NPs to enhance glucose utilization, aiding in blood glucose regulation. The superior performance of CuO NPs A, particularly in glucose uptake at T30 and T120, can be attributed to their smaller size and larger surface area, which enhance their interaction with glucose transporters on the cell

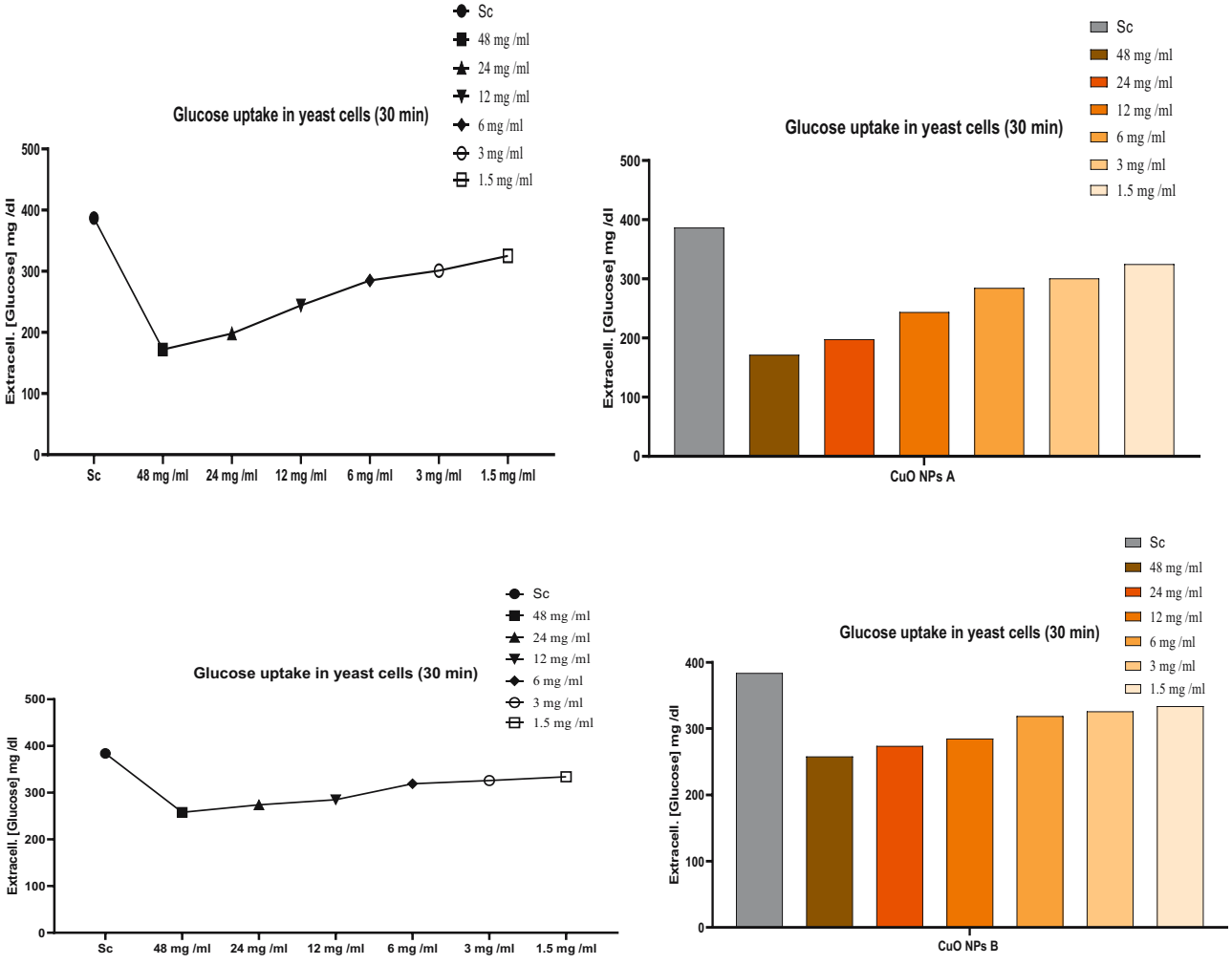

Figure 13: *In vitro* antidiabetic activity of CuO NPs A and CuO NPs B using a yeast cell model represented by extracellular glucose concentration (mg·mL^{-1}) uptake by yeast cells by different concentrations of NPs at 30 min; Sc = yeast of *S. cerevisiae*.

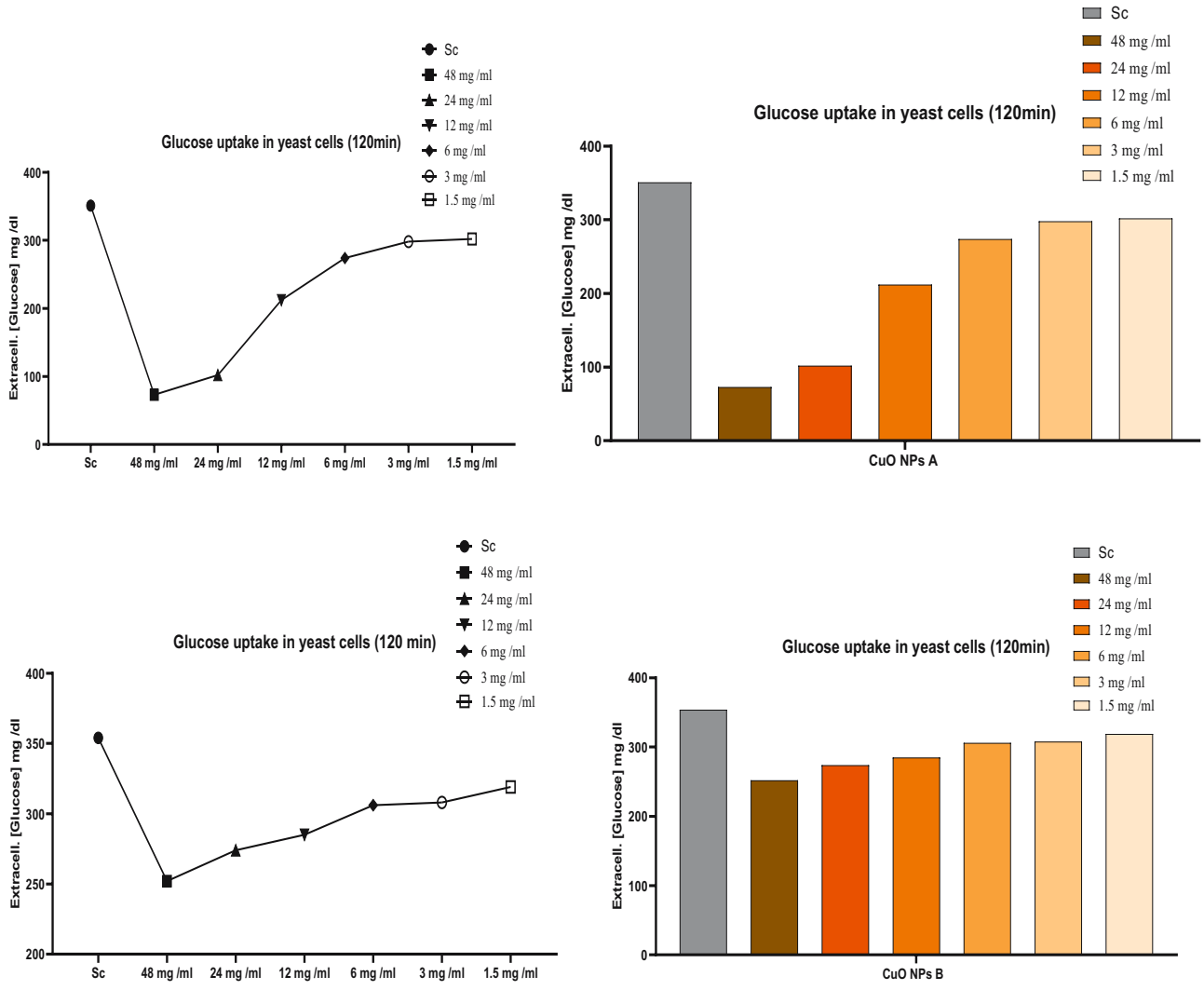

Figure 14: *In vitro* antidiabetic activity of CuO NPs A and CuO NPs B using a yeast cell model represented by extracellular glucose concentration (mg·mL^{-1}) uptake by yeast cells by different concentrations of NPs at times 120 min; Sc = yeast of *Saccharomyces cerevisiae.*

Table 7: *In vitro* antidiabetic activity of CuONPs A and CuONPs B using a yeast cell model represented by extracellular glucose concentration (mg·mL^{-1}) uptake by yeast cells by different concentrations of NPs at 30 min; Sc = yeast of *S. cerevisiae*

Cc. (mg·mL^{-1})	T (T0)	(T30)	(T30)					
	Control		48 mg·mL^{-1}	24 mg·mL^{-1}	12 mg·mL^{-1}	6 mg·mL^{-1}	3 mg·mL^{-1}	1.5 mg·mL^{-1}
CuO NPs A	453	387	172	198	244	285	301	325
CuO NPs B	453	384	258	274	285	319	326	334

Table 8: *In vitro* antidiabetic activity of CuO NPs A and CuO NPs B using a yeast cell model represented by extracellular glucose concentration (mg·mL^{-1}) uptake by yeast cells by different concentrations of NPs at 120 min; Sc = yeast of *S. cerevisiae*

Cc. (mg·mL^{-1})	T (T0)	(T120)	(T120)					
	Control		48 mg·mL^{-1}	24 mg·mL^{-1}	12 mg·mL^{-1}	6 mg·mL^{-1}	3 mg·mL^{-1}	1.5 mg·mL^{-1}
CuO NPs A	453	351	73	102	212	274	298	302
CuO NPs B	453	354	252	274	285	306	308	319

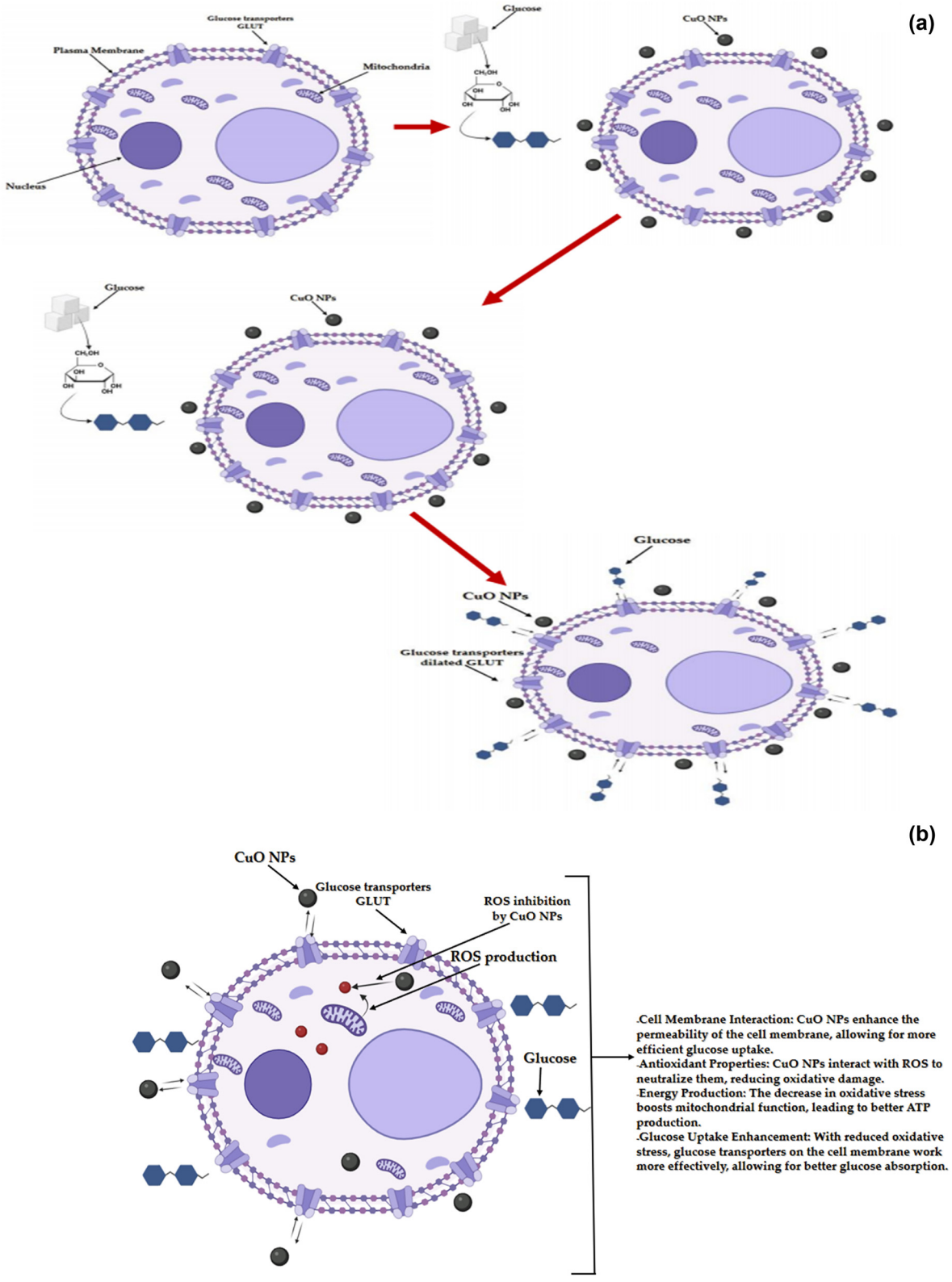

Figure 15: Antidiabetic mechanism of action: (a) Glucose uptake by the cell. (b) Mechanism of inhibition of oxidative stress in the cell by CuO NPs. (c) Mechanism of inhibition of enzymes by CuO NPs. (d) Mechanism of expansion of glucose transporters by CuO NPs.

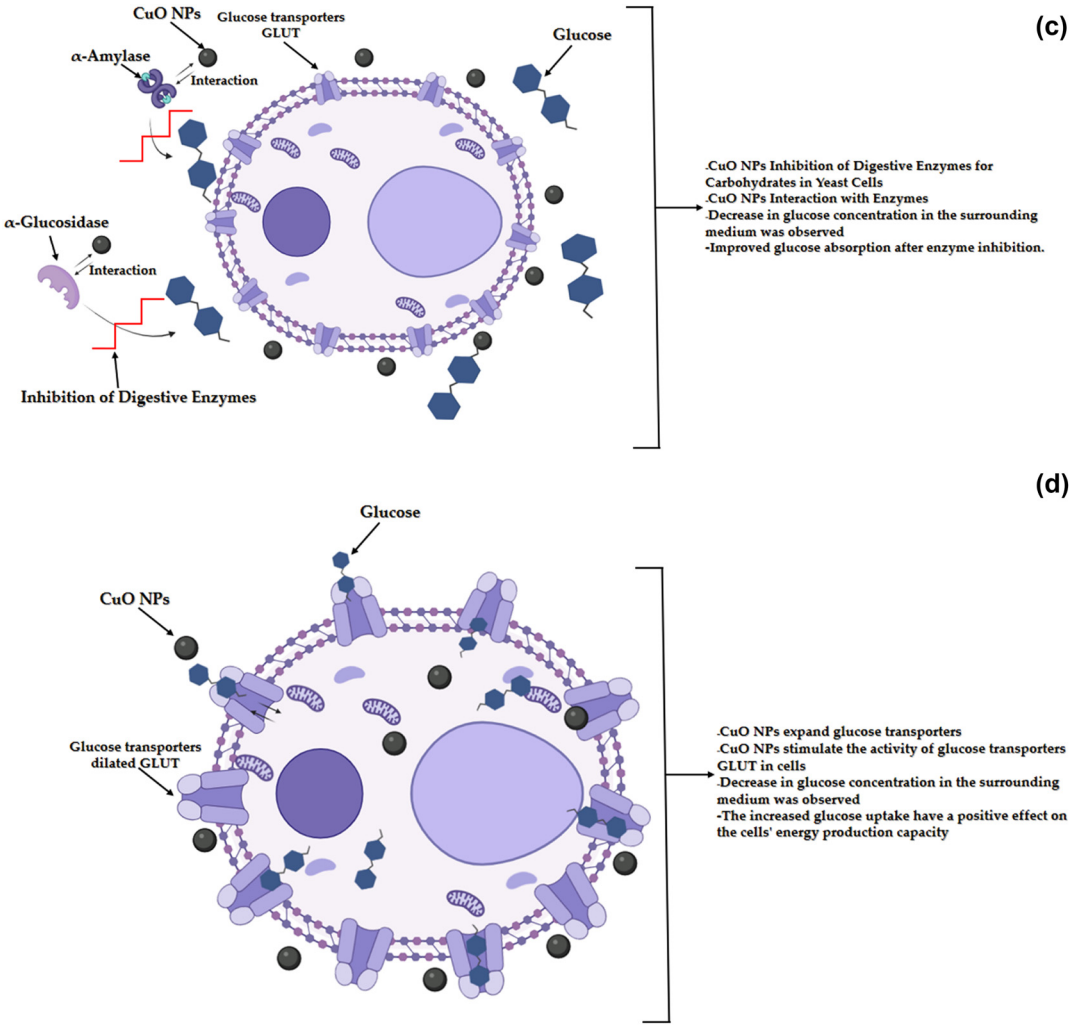

Figure 15: (*Continued*)

membrane, contributing to more efficient glucose absorption and utilization.

The observed increase in glucose uptake in yeast cells treated with CuO NPs can be attributed to several mechanisms, as illustrated in Figure 15. CuO NPs interact with the yeast cell membrane, stimulating the activity of glucose transporters (GLUT) (Figure 15c). These NPs enhance the functionality of glucose transporters, facilitating glucose movement into the cell. This interaction leads to a reduction in extracellular glucose concentration, indicating effective glucose uptake. Enhanced glucose uptake positively contributes to cellular energy production by promoting intracellular glucose utilization [53].

CuO NPs exhibit inhibitory effects on carbohydrate-digesting enzymes such as α-amylase and α-glucosidase (Figure 15b). By inhibiting these enzymes, CuO NPs reduce the breakdown of complex carbohydrates into glucose, thereby limiting the amount of free glucose available in the extracellular medium. This reduction improves the efficiency of glucose transporters in absorbing available glucose into cells, further enhancing glucose uptake and utilization [57].

CuO NPs interact with ROS produced during cellular metabolism (Figure 15a). By neutralizing ROS, these NPs reduce oxidative stress within the cell, which is known to impair glucose transporter activity. The antioxidant properties of CuO NPs help maintain the integrity of GLUT, enhancing their functionality and promoting efficient glucose absorption. Furthermore, reducing oxidative stress improves mitochondrial function, boosting ATP production and enhancing cellular energy metabolism [55].

The results of this study are consistent with recent reports suggesting that NPs can modulate glucose uptake through their interaction with membrane transporters and enzymatic pathways. The ability of CuO NPs to regulate glucose transport and utilization highlights their potential as therapeutic agents for diabetes management [53,54,56].

4 Conclusion

This study successfully demonstrated the green synthesis of CuO NPs using propolis extract, an economical and sustainable raw material priced at €25 per 100 g. The synthesis produced two variants: CuO A and CuO B (calcined). CuO A exhibited superior biological and structural properties, with distinct UV-Vis absorption peaks at 314 and 370 nm, compared to the broader peak at 355 nm for CuO B. Structural analysis revealed spherical morphology for CuO A and star-shaped structures for CuO B, with average crystallite sizes of 68.5 and 74.82 nm, respectively. Biological analyses highlighted exceptional antioxidant activity of CuO A, with an IC_{50} of 0.027 and an AEAC of 2.01, compared to an IC_{50} of 0.052 and an AEAC of 1.76 for CuO B. CuO A also demonstrated stronger antimicrobial activity (MIC: 5–10 $mg{\cdot}mL^{-1}$) and superior glucose-lowering potential in yeast cells, emphasizing its promise as an antidiabetic agent.

Future studies will focus on a more comprehensive evaluation of the pharmacokinetic properties of these NPs *in vivo*. Additionally, toxicity will be assessed both *in vitro* and *in vivo* rather than relying solely on *in silico* methods. Beyond their antibacterial and antioxidant properties, these NPs show potential for applications such as drug delivery systems and environmental remediation.

Acknowledgments: The authors acknowledge and extend their appreciation to the Researchers Supporting Project (Number RSPD2025R709), King Saud University, Riyadh, Saudi Arabia, for supporting this study.

Funding information: This research was supported by King Saud University, Riyadh, Saudi Arabia (Project Number RSPD2025R709).

Author contributions: Conceptualization: A.R. and H.Z.; methodology: R.B.S. and G.R.; validation: AA.; formal analysis: D.C. and M.A.A.; investigation: H.Z. and G.R.; resources: R.B.S.; data curation: D.C. and M.A.A.; writing – original draft: A.R., H.Z., and A.A.; writing – review & editing: R.B.S., G.R., and M.M.; visualization: R.B.S.; supervision: A.R. and R.B.S.; project administration: A.R. and G.R. The authors have read and agreed to the published version of the manuscript.

Conflict of interest: Authors state no conflict of interest.

Data availability statement: All data generated or analyzed during this study are included in this published article.

References

[1] Tavakoli A, Sohrabi M, Kargari A. A review of methods for synthesis of nanostructured metals with emphasis on iron compounds. Chem Pap. 2007;61(3):151–70. doi: 10.2478/s11696-007-0014-7.

[2] Ying S, Guan Z, Ofoegbu PC, Clubb P, Rico C, He F, et al. Green synthesis of nanoparticles: Current developments and limitations. Environ Technol Innov. 2022;26:102336. doi: 10.1016/j.eti.2022.102336.

[3] Ruparelia JP, Chatterjee AK, Duttagupta SP, Mukherji S. Strain specificity in antimicrobial activity of silver and copper nanoparticles. Acta Biomater. 2008;4(3):707–16. doi: 10.1016/j.actbio.2007.11.006.

[4] Ren G, Hu D, Cheng EW, Vargas-Reus MA, Reip P, Allaker RP. Characterisation of copper oxide nanoparticles for antimicrobial applications. Int J Antimicrobial Agents. 2009;33(6):587–90. doi: 10.1016/j.ijantimicag.2008.12.004.

[5] Yoon K-Y, Hoon Byeon J, Park JH, Hwang J. Susceptibility constants of Escherichia coli and Bacillus subtilis to silver and copper nanoparticles. Sci Total Environ. 2007;373(2–3):572–5. doi: 10.1016/j.scitotenv.2006.11.007.

[6] Ijaz F, Shahid S, Khan SA, Ahmad W, Zaman S. Green synthesis of copper oxide nanoparticles using Abutilon indicum leaf extract: Antimicrobial, antioxidant and photocatalytic dye degradation activitie. Trop J Pharm Res. 2017;16(4):743–53. doi: 10.4314/tjpr.v16i4.2.

[7] Dadkhah M, Tulliani J-M. Green synthesis of metal oxides semiconductors for gas sensing applications. Sensors (Basel, Switzerland). 2022;22(13):4669. doi: 10.3390/s22134669.

[8] Yusop HM, Ismail WNW, Zulkifli NFM, Tajuddin SN. Effect of CuO antibacterial coating on cotton, polyester, and blend wool fabrics. Biointerface Res Appl Chem. 2023. doi: 10.33263/BRIAC136.591.

[9] Jini D, Sharmila S, Anitha A, Pandian M, Rajapaksha R. In vitro and in silico studies of silver nanoparticles (AgNPs) from Allium sativum against diabetes. Sci Rep. 2022;12(1):22109. doi: 10.1038/s41598-022-24818-x.

[10] Alkaladi A, Abdelazim AM, Afifi M. Antidiabetic activity of zinc oxide and silver nanoparticles on streptozotocin-induced diabetic rats. Int J Mol Sci. 2014;15(2):2015–23. doi: 10.3390/ijms15022015.

[11] Siddiqi KS, Ur Rahman A, Tajuddin T, Husen A. Properties of zinc oxide nanoparticles and their activity against microbes. Nanoscale Res Lett. 2018;13:141. doi: 10.1186/s11671-018-2532-3.

[12] Hasnidawani JN, Azlina HN, Norita H, Bonnia NN, Ratim S, Ali ES. Synthesis of ZnO nanostructures using sol-gel method. Procedia Chem. 2016;19:211–6. doi: 10.1016/j.proche.2016.03.095.

[13] Makarov VV, Love AJ, Sinitsyna OV, Makarova SS, Yaminsky IV, Taliansky ME, et al. "Green" nanotechnologies: Synthesis of metal nanoparticles using plants. Acta Naturae (англоязычная версия). 2014;6(1(20)):35–44. doi: 10.32607/20758251-2014-6-1-35-44.

[14] Barbarić M, Mišković K, Bojić M, Lončar MB, Smolčić-Bubalo A, Debeljak Z, et al. Chemical composition of the ethanolic propolis extracts and its effect on HeLa cells. J Ethnopharmacol. 2011;135(3):772–8. doi: 10.1016/j.jep.2011.04.015.

[15] López BG, Schmidt EM, Eberlin MN, Sawaya AC. Phytochemical markers of different types of red propolis. Food Chem. 2014;146:174–80. doi: 10.1016/j.foodchem.2013.09.063.

[16] Sforcin JM. Propolis and the immune system: A review. J Ethnopharmacol. 2007;113(1):1–14. doi: 10.1016/j.jep.2007.05.012.

[17] Gatea F, Teodor ED, Seciu AM, Covaci OI, Mănoiu S, Lazăr V, et al. Antitumour, antimicrobial and catalytic activity of gold nanoparticles synthesized by different pH propolis extracts. J Nanopart Res. 2015;17:1–13. doi: 10.1007/s11051-015-3127-x.

[18] Righi AA, Alves TR, Negri G, Marques LM, Breyer H, Salatino A. Brazilian red propolis: Unreported substances, antioxidant and antimicrobial activities. J Sci Food Agric. 2011;91(13):2363–70. doi: 10.1002/jsfa.4468.
[19] Al-Fakeh MS, Osman S, Gassoumi M, Rabhi M, Omer M. Biosynthesis and characterization of Saudi propolis-mediated silver nanoparticles and their biological properties. Open Phys. 2021;19(1):753–7. doi: 10.1515/phys-2021-0091.
[20] Abdelsattar AS, Eid A, Rezk N, Hussein AH, El-Shibiny A. Biosynthesis of gold nanoparticles using ethanolic propolis extract for methylene blue and Rhodamine-B removal. Mater Lett. 2022;327:133060. doi: 10.1016/j.matlet.2022.133060.
[21] Al-Fakeh MS, Osman S, Gassoumi M, Rabhi M, Omer M. Characterization, antimicrobial and anticancer properties of palladium nanoparticles biosynthesized optimally using Saudi propolis. Nanomaterials (Basel, Switz). 2021;11(10):2666. doi: 10.3390%2Fnano11102666.
[22] Hatami R, Javadi A, Jafarizadeh-Malmiri H. Effectiveness of six different methods in green synthesis of selenium nanoparticles using propolis extract: Screening and characterization. Green Process Synth. 2020;9(1):685–92. doi: 10.1515/gps-2020-0065.
[23] Mendez-Pfeiffer P, Ballesteros-Monrreal MG, Gaona-Ochoa J, Juarez J, Gastelum-Cabrera M, Montaño-Leyva B, et al. Biosynthesis of silver nanoparticles using seasonal samples of Sonoran desert propolis: Evaluation of its antibacterial activity against clinical isolates of multi-drug resistant bacteria. Pharmaceutics. 2022;14(9):1853. doi: 10.3390/pharmaceutics14091853.
[24] Šuran J, Cepanec I, Mašek T, Radić B, Radić S, Tlak Gajger I, et al. Propolis extract and its bioactive compounds—From traditional to modern extraction technologies. Molecules. 2021;26(10):2930. https://www.mdpi.com/1420-3049/26/10/2930.
[25] Kouadri I, Rebiai A, Hemmami H, Seghir BB, Zeghoud S, Berra D, et al. Impact of geographic variation on the chemical composition and antioxidant activity of Algerian propolis. Appl Biol Sahar Areas. 2021;3(7):27–41. https://www.researchgate.net/profile/Bachir-Ben-Seghir/publication/357469596_Impact_of_geographic_variation_on_the_chemical_composition_and_antioxidant_activity_of_Algerian_propolis/links/6256b35f328abe6281540b0b/Impact-of-geographic-variation-on-the-chemical-composition-and-antioxidant-activity-of-Algerian-propolis.pdf.
[26] Malaikozhundan B, Lakshmi VN, Krishnamoorthi R. Copper oxide nanoparticles using Mentha spicata leaves as antibacterial, antibiofilm, free radical scavenging agent and efficient photocatalyst to degrade methylene blue dyes. Mater Today Commun. 2022;33:104348. doi: 10.1016/j.mtcomm.2022.104348.
[27] Desai R, Mankad V, Gupta S, Jha P. Size distribution of silver nanoparticles: UV-visible spectroscopic assessment. Nanosci Nanotechnol Lett. 2012;4(1):30–4. doi: 10.1166/nnl.2012.1278.
[28] Torres-Rivero K, Bastos-Arrieta J, Fiol N, Florido A. Metal and metal oxide nanoparticles: an integrated perspective of the green synthesis methods by natural products and waste valorization: applications and challenges. Compr Anal Chem. 2021;94:433–69. doi: 10.1016/bs.coac.2020.12.001.
[29] Hurma T. Structural optical and electrical characterization of nanoparticle B doped ZnS films. Mater Sci Pol. 2019;37(4):599–606. doi: 10.2478/msp-2019-0072.
[30] Djamila B, Eddine LS, Abderrhmane B, Nassiba A, Barhoum A. In vitro antioxidant activities of copper mixed oxide (CuO/Cu2O) nanoparticles produced from the leaves of Phoenix dactylifera L. Biomass Convers Biorefin. 2022;14:6567–80. doi: 10.1007/s13399-022-02743-3.
[31] Benzie IF, Strain JJ. The ferric reducing ability of plasma (FRAP) as a measure of "antioxidant power": the FRAP assay. Anal Biochem. 1996;239(1):70–6. doi: 10.1006/abio.1996.0292.
[32] Ardestani A, Yazdanparast R. Inhibitory effects of ethyl acetate extract of Teucrium polium on in vitro protein glycoxidation. Food Chem Toxicol. 2007;45(12):2402–11. doi: 10.1016/j.fct.2007.06.020.
[33] Balouiri M, Sadiki M, Ibnsouda SK. Methods for in vitro evaluating antimicrobial activity: A review. J Pharm Anal. 2016;6(2):71–9. doi: 10.1016/j.jpha.2015.11.005.
[34] Cirillo VP. Mechanism of glucose transport across the yeast cell membrane. J Bacteriol. 1962;84(3):485–91.
[35] Kurek-Górecka A, Rzepecka-Stojko A, Górecki M, Stojko J, Sosada M, Swierczek-Zieba G. Structure and antioxidant activity of polyphenols derived from propolis. Molecules. 2013;19(1):78–101. doi: 10.3390/molecules19010078.
[36] Varthamanan J. Anti cancer activity of silver nano particles biosynthesized using stingless bee propolis (Tetragonula iridipennis) of Tamilnadu. Asian J Biomed Pharm Sci. 2015;5(40):30. doi: 10.15272/ajbps.v4i40.654.
[37] Nasrollahzadeh M, Sajadi SM, Rostami-Vartooni A, Hussin SM. Green synthesis of CuO nanoparticles using aqueous extract of Thymus vulgaris L. leaves and their catalytic performance for N-arylation of indoles and amines. J Colloid Interface Sci. 2016;466:113–9. doi: 10.1016/j.jcis.2015.12.018.
[38] Das D, Nath BC, Phukon P, Dolui SK. Synthesis and evaluation of antioxidant and antibacterial behavior of CuO nanoparticles. Colloids Surf B Biointerfaces. 2013;101:430–3. doi: 10.1016/j.colsurfb.2012.07.002.
[39] Galil MA, Osman SO, Moharem AS, Alqubati M, Saif EA, Omer MM. Optimal biosynthesis and characterization of broad-spectrum antibacterial cupric oxide nanoparticles using bee glue. Moroccan J Chem. 2023;11(4):1203–20. doi: 10.48317/IMIST.PRSM/morjchem-v11i04.41345.
[40] Ibrahim N, Jamil Zakaria A, Ismail Z, Ahmad Y, Suryati Mod K. Application of GCMS and FTIR fingerprinting in discriminating two species of Malaysian stingless bees propolis. Int J Eng Technol. 2018;7:106–12. doi: 10.14419/ijet.v7i4.43.25828.
[41] Hajinezhad S, Razavizadeh BM, Niazmand R. Study of antimicrobial and physicochemical properties of LDPE/propolis extruded films. Polym Bull. 2020;77:4335–53. https://link.springer.com/article/10.1007/s00289-019-02965-y.
[42] Hegazi AG, El-Houssiny AS, Fouad EA. Egyptian propolis 14: Potential antibacterial activity of propolis-encapsulated alginate nanoparticles against different pathogenic bacteria strains. Adv Nat Sci: Nanosci Nanotechnol. 2019;10(4):045019. doi: 10.1088/2043-6254/ab52f4.
[43] Davari A, Hakimzadeh V, Mahdian E, Shahidi-Noghabi M. Synthesis and characterization of copper oxide nanoparticles using aqueous extract of iranian violaceae flower. FST. 2021. doi: 10.15673/fst.v15i3.2178.
[44] Amaliyah S, Pangesti DP, Masruri M, Sabarudin A, Sumitro SB. Green synthesis and characterization of copper nanoparticles using Piper retrofractum Vahl extract as bioreductor and capping agent. Heliyon. 2020;6(8):04636. doi: 10.1016/j.heliyon.2020.e04636.
[45] Sarkar J, Chakraborty N, Chatterjee A, Bhattacharjee A, Dasgupta D, Acharya K. Green synthesized copper oxide nanoparticles

ameliorate defence and antioxidant enzymes in Lens culinaris. Nanomaterials (Basel, Switz). 2020;10(2):312. doi: 10.3390/nano10020312.

[46] Min X, Yang Q, Zhou P. Effects of nano-copper oxide on antioxidant function of copper-deficient Kazakh sheep. Biol Trace Elem Res. 2022;200(8):3630–7. doi: 10.1007/s12011-021-02975-w.

[47] Strompfová V, Štempelová L, Wolaschka T. Antibacterial activity of plant-derived compounds and cream formulations against canine skin bacteria. Vet Res Commun. 2024;48(3):1459–70. https://link.springer.com/article/10.1007/s11259-024-10324-0.

[48] Heli H, Tondro G, Sattar Ahmady N, Dehdari Vais R, VeisiKahreh H. Nanoparticles of copper and copper oxides: Synthesis and Determination of antibacterial activity. J Kerman Univ Med Sci. 2017;24(2):166–70. https://jkmu.kmu.ac.ir/article_46786.html.

[49] Zain NM, Stapley AG, Shama G. Green synthesis of silver and copper nanoparticles using ascorbic acid and chitosan for antimicrobial applications. Carbohydr Polym. 2014;112:195–202. https://www.sciencedirect.com/science/article/abs/pii/S0144861714005591.

[50] Jeziórska R, Zielecka M, Gutarowska B, Żakowska Z. High-density polyethylene composites filled with nanosilica containing immobilized nanosilver or nanocopper: Thermal, mechanical, and bactericidal properties and morphology and interphase characterization. Int J Polym Sci. 2014;2014(1):183724. https://onlinelibrary.wiley.com/doi/full/10.1155/2014/183724.

[51] Effenberger FB, Sulca MA, Machini MT, Couto RA, Kiyohara PK, Machado G, et al. Copper nanoparticles synthesized by thermal decomposition in liquid phase: the influence of capping ligands on the synthesis and bactericidal activity. J Nanopart Res. 2014;16:1–10. https://link.springer.com/article/10.1007/s11051-014-2588-7.

[52] Hajipour MJ, Fromm KM, Ashkarran AA, Jimenez de Aberasturi D, de Larramendi IR, Rojo T, et al. Antibacterial properties of nanoparticles. Trends Biotechnol. 2012;30(10):499–511. https://www.cell.com/trends/biotechnology/abstract/S0167-7799(12)00095-9.

[53] Pitchaipillai R, Ponniah T. In vitro antidiabetic activity of ethanolic leaf extract of bruguiera Cylindrica L.–glucose uptake by yeast cells method. Int Biol Biomed J. 2016;2(4):171–5. http://ibbj.org/article-1-92-en.html.

[54] Pulivarthi V, Josthna P, Naidu C. In vitro antidiabetic activity by glucose uptake of yeast cell assay and antioxidant potential of Annona Reticulata L. leaf extracts. Int J Pharm Sci Drug Res. 2020. https://pesquisa.bvsalud.org/portal/resource/pt/sea-206310.

[55] Maier A, Völker B, Boles E, Fuhrmann GF. Characterisation of glucose transport in Saccharomyces cerevisiae with plasma membrane vesicles (countertransport) and intact cells (initial uptake) with single Hxt1, Hxt2, Hxt3, Hxt4, Hxt6, Hxt7 or Gal2 transporters. FEMS Yeast Res. 2002;2(4):539–50. https://academic.oup.com/femsyr/article/2/4/539/551853.

[56] Teusink B, Diderich JA, Westerhoff HV, van Dam K, Walsh MC. Intracellular glucose concentration in derepressed yeast cells consuming glucose is high enough to reduce the glucose transport rate by 50%. J Bacteriol. 1998;180(3):556–62. https://journals.asm.org/doi/full/10.1128/jb.180.3.556-562.1998.

[57] Faiyaz Ahmed FA, Sudha Sairam SS, Asna Urooj AU. Effect of various ayurvedic formulations and medicinal plants on carbohydrate hydrolyzing enzymes and glucose uptake by yeast cells-an in vitro study. J Pharm Res. 2009. https://www.researchgate.net/publication/309476222_Effect_of_various_Ayurvedic_formulations_and_medicinal_plants_on_carbohydrate_hydrolyzing_enzymes_and_glucose_uptake_by_yeast_cells-an_in_vitro_study.